Fundamental Methods to Measure the Orbital Angular Momentum of Light

Berkhout, G.C.G.

CHAPTER 7

Measuring orbital angular momentum superpositions of light by mode transformation

In chapter 6 we reported on a method for measuring orbital angular momentum (OAM) states of light based on the transformation of helically phased beams to tilted plane waves. Here we consider the performance of such a system for superpositions of OAM states by measuring the modal content of noninteger OAM states and beams produced by a Heaviside phase plate.

G. C. G. Berkhout, M. P. J. Lavery, M. J. Padgett, and M. W. Beijersbergen, *Measuring orbital angular momentum superpositions of light by mode transformation,* Optics Letters **36**, 1863 (2011).

7.1 Introduction

Ever since it was first described that a light beam containing an optical vortex, $\exp(i\ell\phi)$, carries an orbital angular momentum (OAM) of $\ell\hbar$ per photon for integer ℓ [1], this subject has drawn significant interest [25]. In addition to its fundamental properties, the application of OAM in optical communication [33] has been studied.

Optical vortices occur in higher-order laser modes; can be created by means of a mode converter [63], spiral phase plate [5] or fork hologram [52]; and can also be made by encoding the appropriate hologram on a spatial light modulator (SLM) [47]. In addition, optical vortices occur in caustics [64] and speckle patterns [8].

Although creating optical vortices is relatively straightforward, measuring their topological charge, ℓ, is not. Several methods are being used, ranging from interference [15], diffraction [27, 55], holograms [54], q-plates [65] and interferometers [13] to mode specific detection [29]. All these methods have significant disadvantages; they either work only for many photons in the same state, have low throughput, are technically very challenging or can detect only one state at a time.

Recently we have described a system comprising two custom, static optical components that allows simultaneous detection of many different OAM modes (chapter 6). The system is based on performing a Cartesian to log-polar optical transformation [58] that transforms the helically phased beam around an optical vortex into a tilted plane wave. Optical vortices with different topological charges are transformed into plane waves with a different tilt that, in turn, are focused to different positions in the focal plane of a lens. The topological charge is thus encoded in the lateral position of the spot; all radial information is encoded in the orthogonal axis in the focal plane. Because of the design of the optical transformation, the spots will slightly overlap, which limits the use of the system for single photon applications. This could be resolved by changing the design of the two custom components, at the expense of making the optical design more complex [66].

The main advantage of the mode-transforming system is its ability to detect multiple modes at the same time. A spectrum of optical vortices can be generated by spontaneous parametric downconversion [67] or by phase plates, such as noninteger spiral phase plates [68] and angular sector phase plates [69]. A misaligned beam also gives rise to a spectrum of OAM states [70]. Finally, one can create arbitrary superpositions of orbital angular momentum states by displaying the correct superposition of spiral phase plates as a hologram on the SLM.

The modal content of any superposition can be directly derived from the positions and relative intensities of the spots on a detector in the focal plane of the mode sorter. For potential single-photon applications, the position where the photon hits the detector is statistically determined by the input superposition.

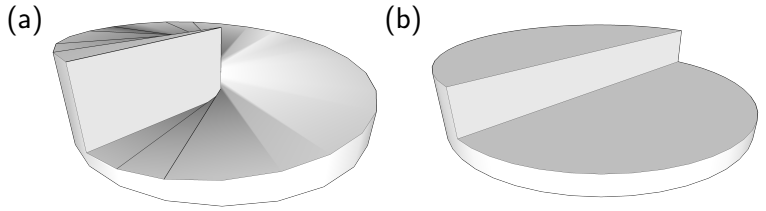

Figure 7.1: Schematic drawing of (a) a spiral phase plate and (b) a Heaviside phase plate.

7.2 Theory

In this chapter, we measure the modal content of noninteger OAM states and beams produced by a Heaviside phase plate (see figure 7.1). Following [69], we can calculate these modal contents theoretically, neglecting the radial dependence. A general superposition of optical vortex states is given by

$$A(\phi) = \sum_{m_\ell} \lambda_{m_\ell} A_{m_\ell}(\phi), \tag{7.1}$$

where $A_{m_\ell}(\phi) = \frac{1}{\sqrt{2\pi}} e^{im_\ell \phi}$ are the normalized vortex states. The modal coefficients for an arbitrary superposition can be found by

$$\lambda_{m_\ell} = \frac{1}{\sqrt{2\pi}} \int_0^{2\pi} e^{-im_\ell \phi} A(\phi) d\phi. \tag{7.2}$$

We further define $\gamma_{m_\ell} = |\lambda_{m_\ell}|^2$. The normalization of the vortex states guarantees that $\sum_{m_\ell} \gamma_{m_\ell} = 1$.

A noninteger OAM state is given by $\exp(i\ell\phi)$, where ℓ is the non-integer topological charge. From equation 7.2, we calculate that

$$\lambda_{m_\ell} = \mathrm{sinc}((\ell - m_\ell)\pi) e^{i(\ell - m_\ell)\pi}, \tag{7.3}$$

which reduces to $\lambda_{m_\ell} = \delta_{m_\ell,\ell}$ if ℓ becomes integer, where $\delta_{i,j}$ is the Kronecker delta.

In addition to the noninteger spiral phase plate, we measure the modal content of the field behind a Heaviside phase plate, which is characterised by a phase step of π between the two halfs of the phase plate, resulting in a spectrum as defined in [69].

7.3 Experiment

A schematic overview of the experimental setup is shown in figure 7.2. Although it is possible to manufacture all required optical components from glass or plastic, we encode them on three SLMs, which can be used to imprint any spatially varying phase to a beam.

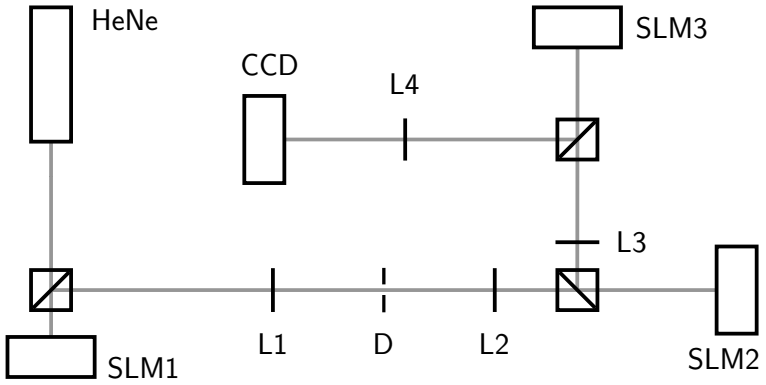

Figure 7.2: Schematic overview of the setup. See text for details.

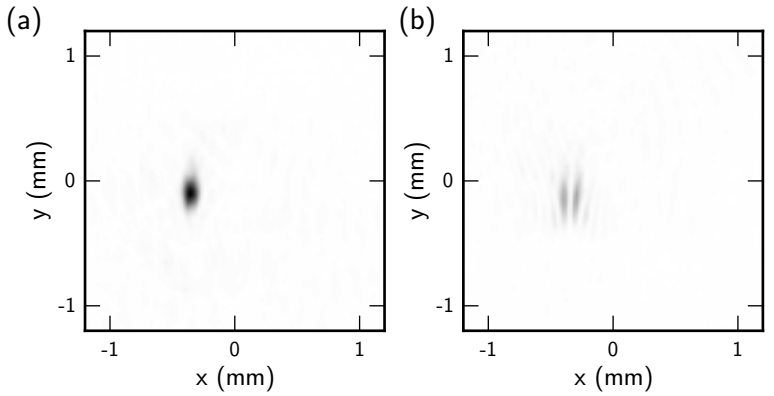

Figure 7.3: CCD images for an equal superposition of two modes ($m_\ell = -1$ and $m_\ell = 0$) with a relative phase of (a) $\psi_i = 0$ and (b) $\psi_i = \pi$. Both images are scaled to the peak intensity of the image shown in (a). The color scale is inverted for clarity.

SLM1 is used to create all input states, either by encoding a noninteger or Heaviside phase plate or by encoding an arbitrary superposition of spiral phase plates. The input states are imaged onto SLM2 using two lenses (L1 and L2) and a diaphragm (D) to filter out the correct diffraction order. The mode sorter, whose phase profiles are described in chapter 6, comprises two SLMs (SLM2 and SLM3), together with a lens (L3). A lens (L4) is used to focus the output of the mode sorter onto a CCD camera. We use beam splitters to ensure perpendicular incidence on all SLMs.

7.4 Results

As described above, the position of the focussed spot on the CCD camera depends on the OAM state of the input beam. For a superposition, we expect to see more than

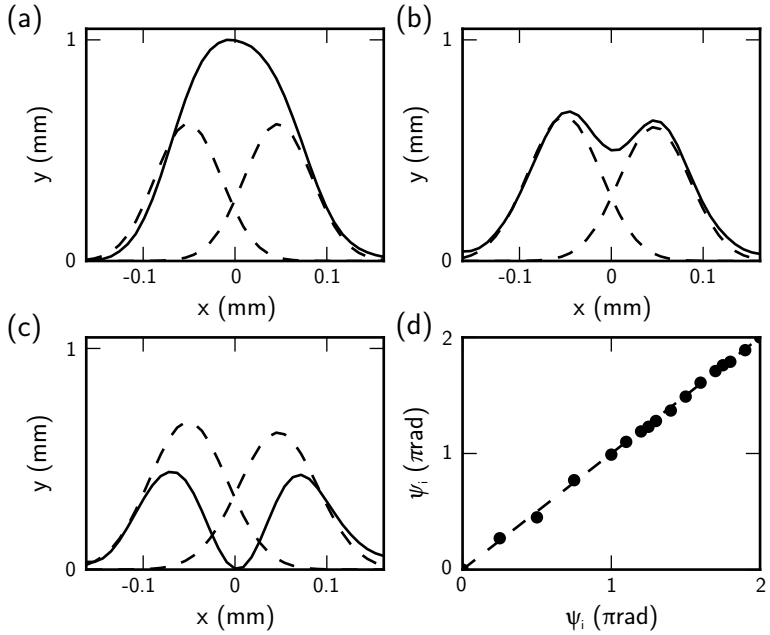

Figure 7.4: Summed CCD images with a relative phase of (a) $\psi_i = 0$ (corresponding to figure 7.3 (a)), (b) $\psi_i = \pi/2$ and (c) $\psi_i = \pi/2$ (corresponding to figure 7.3 (b)) (solid lines). The dashed lines show the fitted peaks of the individual modes. (d) The measured relative phase, ψ_m, as returned by the fit versus the input relative phase, ψ_i, as set on SLM1.

one spot with relative intensities, depending on the modal content (see figure 7.3 for typical examples). Since there is no extra information in the y axis of the CCD images, we sum them over the rows to increase the signal-to-noise ratio. We extract the relative amplitudes from these summed images by fitting a sum of the theoretically expected peaks for the individual modes. In the fitting routine, we allow some margin in the peak position and the peak width to compensate for possible experimental errors.

We study the output of the mode sorter for an equal superposition of two modes ($m = -1$ and $m = 0$) with changing relative phase. Figure 7.4 (a-c) show typical summed images. Note that one can only see the effect of the relative phase in the regions where the peaks overlap and interfere constructively or destructively, depending on the relative phase. In addition, figure 7.4 shows the fitted peaks of both modes as dashed curves. The fit returns the amplitudes of the peaks and the relative phase between the states. Figure 7.4 (d) shows the fitted relative phases for a number of input phases, as set on SLM1. This figure demonstrates that the relative phase between the states in conserved by the transformation. The output relative phases also depend on the angular orientation of the mode sorter around the optical axis. All data are corrected for this orientation.

Figure 7.5 (a-e) shows the modal decomposition for noninteger OAM states, both

theoretical as calculated from equation 7.3 (black), and exprimental (gray), where ℓ is varied between $\ell = -1$ and $\ell = 0$. One can clearly see that the peak shifts from $m = -1$ to $m = 0$. For noninteger values of ℓ, the spectrum broadens. Figure 7.5 (f) shows the results for a Heaviside phase plate. The results of the fits are qualitatively in good agreement with the theoretically predicted values.

7.5 Discussion

We have shown that mode transformation preserves the relative phase between input states and that this relative phase can be measured in regions where the peaks of two transformed modes overlap, which experimentally works fine if the modes have $\Delta m = 1$. An alternative way to measure the relative phase would be interfering the output of the mode sorter with a flat wave front, increasing the complexity of the system. The fact that the mode transformation separates the modes spatially and preserves coherence, could be used to manipulate modes in a superposition.

An important application of a optical vortex mode sorter is in optical communication. The optical vortex states span a higher-dimensional basis, which could be used to encode information in. As shown in this chapter, our mode sorter could be used to decode the information that is in superpositions of neighboring optical vortex states.

7.6 Conclusion

In conclusion, we have shown the principle that our previously presented mode sorter can be used to determine the modal content of OAM superpositions in a single, practical measurement. This system can be used as a decoder in higher-dimensional optical communication schemes based on OAM states.

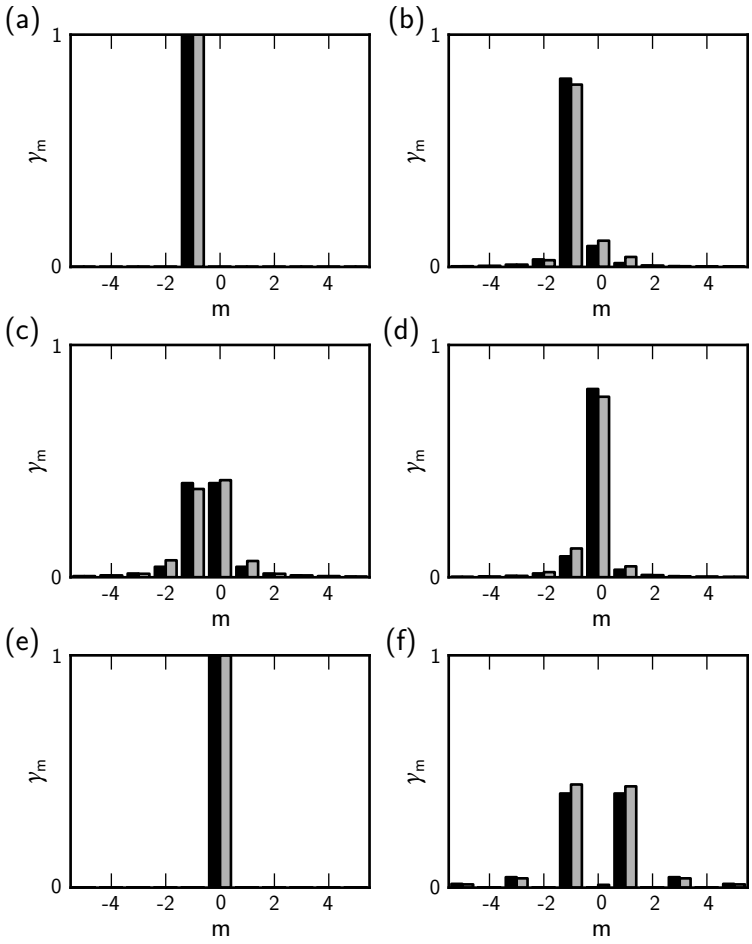

Figure 7.5: Modal decomposition of a non-integer OAM state with (a) $\ell = -1$, (b) $\ell = -\frac{3}{4}$, (c) $\ell = -\frac{1}{2}$, (d) $\ell = -\frac{1}{4}$, (e) $\ell = 0$ and (f) the beam produced by a Heaviside phase plate. Theoretical data is shown in black, experimental data in grey.